Palaeogeography, Palaeoclimatology, Palaeoecology 617 (2023) 111474

Contents lists available at ScienceDirect

Palaeogeography, Palaeoclimatology, Palaeoecology

journal homepage: www.elsevier.com/locate/palaeo

Tree-ring δ^{18}Ocellulose variations in two *Nothofagus* species record large-scaleclimatic signals in the South American sector of the Southern Ocean

Pamela Soto-Rogel [a,b,c,*], Juan Carlos Aravena [b,c], Ricardo Villalba [c,d], Wolfgang Jens-Henrik Meier [a], Jussi Grießinger [a]

[a] Institute of Geography, Friedrich-Alexander-Universität Erlangen-Nürnberg, 91058 Erlangen, Germany
[b] Centro de Investigación GAIA Antártica, University of Magallanes (UMAG), Punta Arenas 6200000, Chile
[c] Cape Horn International Center (CHIC), Puerto Williams 6350000, Chile
[d] Instituto Argentino de Nivología, Glaciología y Ciencias Ambientales (IANIGLA-CONICET), Mendoza 5500, Argentina

ARTICLE INFO

Editor: H Falcon-Lang

Keywords:
Tree-ring δ^{18}O
Nothofagus betuloides
Nothofagus pumilio
Antarctic Oscillation (AAO)
Amundsen Sea Low (ASL)
Southernmost South America (SSA)

ABSTRACT

In recent decades, southernmost South America (50–56° S) has experienced marked climate change (regional warming, decreased precipitation, reduced snow cover, and increased frequency of heat waves) related to variations in atmospheric circulation over varied timescales. In this paper, we develop oxygen isotopes from tree-ring cellulose ($\delta^{18}O_{TRC}$) as a proxy for climate and atmospheric circulation in order to extend the regional meteorological record to deeper time intervals. Our work focuses on *Nothofagus* forests in two areas: (i) deciduous *N. pumilio* forest in the steppe transition zone near Punta Arenas and (ii) humid evergreen *N. betuloides* forest in the Navarino Island region. To investigate the potential for reconstructing palaeoclimate, $\delta^{18}O_{TRC}$ variations were correlated with local climate parameters as well as regional (Amundsen Sea Low, ASL) and hemispheric (Antarctic Oscillation, AAO) atmospheric circulation modes for the last 60 years. *N. betuloides* $\delta^{18}O_{TRC}$ variations show an overall positive trend, indicating isotopic enrichment over the study period, whereas no trend is recorded for the *N. pumilio* record. The strongest relationships with climate, together with the widest spatial representativeness, occur in the *N. betuloides* chronology during the growing season (spring to austral summer) and extend spatially from mid to high latitudes. In contrast, the sensitivity of the records is limited to summer months, and spatial correlations are much more limited. In addition, the *N. betuloides* record shows greater potential for reconstructing local climate features such as soil water ($r = -0.76$), wind speed ($r = 0.69$), and precipitation ($r = -0.66$), as well as regional (ASL, $r = -0.80$) and hemispheric (AAO, $r = 0.77$) patterns of extratropical atmospheric circulation. Overall, we conclude that the *N. betuloides* record represents the most valuable tree-ring climate proxy for southernmost South America over past centuries.

1. Introduction

Openly exposed to the westerly winds, the southernmost part of South America, including southern Patagonia, Tierra del Fuego, and its adjacent islands, constitutes the most extensive portion of emerged land in the mid-latitude Southern Hemisphere. Since past and present climate variability in southernmost South America (SSA, 50–56° S) is not well documented, paleoclimatic studies in this region provide an opportunity to advance our understanding of mid-latitude climates and to establish the extent to which present-day climate is unusual in the context of local and regional natural climatic variability.

Despite the scarce available information, substantial climatic changes have been documented in recent decades in SSA. A significant warming of 0.73 °C between 1960 and 2010 has been recorded at Punta Arenas at 53° S (Carrasco, 2013). This warming has been concurrent with an increase in the frequency of heat waves in response to more frequent subtropical warm air masses reaching higher latitudes in South America (Jacques-Coper et al., 2016). A 19% reduction in snow cover over the period 1972–2016 (45 years) has also been reported for the Brunswick Peninsula, west of Punta Arenas. This snow cover decline has

* Corresponding author at: Institute of Geography, Friedrich-Alexander-Universität Erlangen-Nürnberg, 91058 Erlangen, Germany.
E-mail addresses: pamela.soto.rogel@fau.de (P. Soto-Rogel), juan.aravenadonaire@gmail.com (J.C. Aravena), ricardo@mendoza-conicet.gob.ar (R. Villalba), wolfgang.jh.meier@fau.de (W.J.-H. Meier), jussi.griessinger@fau.de (J. Grießinger).

https://doi.org/10.1016/j.palaeo.2023.111474
Received 29 September 2022; Received in revised form 21 February 2023; Accepted 24 February 2023
Available online 28 February 2023

been attributed to long-term warming during the autumn-winter season (April–September) (Aguirre et al., 2018). Consistently, summer precipitation records in Punta Arenas show a substantial negative trend over the last three decades (González-Reyes et al., 2017; Soto-Rogel et al., 2020).

The persistent trends in the average climate and the increase in extreme weather events during the last decades in South America are closely related to the interannual to decadal-scale climate variability, modulated by the El Niño-Southern Oscillation (ENSO, Aceituno, 1988), the Antarctic Oscillation (AAO, Garreaud et al., 2009), the Pacific Decadal Oscillation (PDO; Villalba et al., 2003; Vuille et al., 2015) and the South Pacific Pressure Dipole (Garreaud et al., 2021), among other modes of climate variability. The AAO, also known as the Southern Annular Mode (SAM), is the dominant mode of climate variability in the Southern Hemisphere related to changes in the strength and latitudinal position of the polar jet around Antarctica (Marshall, 2003). The AAO index is a measure of the variations in the meridional pressure gradient in the mid-latitudes of the Southern Hemisphere (Fogt and Marshall, 2020). In recent decades, the AAO index has shown a predominantly positive trend, associated with warmer hemispheric temperatures and Antarctic stratospheric ozone depletion (Polvani et al., 2011). This steady trend, especially during the summer, has induced the movement of the Southern Hemisphere westerly winds (SHWW) towards higher latitudes. Consequently, precipitation in the western mid-latitude sector of South America has decreased as moisture transport from the Pacific to the continent has been reduced in recent decades (Garreaud et al., 2013, 2021).

Since the 1980s, sea level pressure (SLP) has been decreasing in the Amundsen-Bellingshausen Sea (West Antarctic coast) and increasing in the mid-latitudes of the South Pacific, consequently intensifying the pressure gradient across the region (Fogt et al., 2012; Garreaud et al., 2021). The observed trends in the SLP, which are typically stronger in the austral winter, are associated with recently recorded climate changes in West Antarctica and South America (Raphael et al., 2016; Garreaud et al., 2021). Hosking et al. (2013) presented a set of climatological indices to characterize the dynamics of the Amundsen-Bellingshausen Sea (ASL) pressure low. Variations in the ASL are associated with global and hemispheric modes of climate variability (Turner et al., 2013; Raphael et al., 2016). Atmospheric variability in the Amundsen-Bellingshausen region, which is the highest in the Southern Hemisphere, is significantly related to the AAO and ENSO. Since the phase changes of the AAO result in mass exchange between the mid-and high latitudes of the Southern Hemisphere, the sea level pressure in the ASL is strongly influenced by the phase of the AAO. In the positive phase of the AAO, sea level pressure anomalies are negative at high latitudes, inducing a stronger polar jet in the troposphere and an increase in the zonal wind in the ASL region. During the period 1979–2008, the ASL low in January deepened by 1.7 hPa dec-1 in response to the persistent positive trend in the AAO (Turner et al., 2013). Raphael et al. (2016) reported that a significant relationship has been observed between the longitudinal position of the ASL and the zonal wind speed over the Southeast Pacific between 40° and 50° S. Moreover, Westerly winds are weaker when the ASL is located further west (Raphael et al., 2016). Despite these advances in the understanding of ASL dynamics, the influence of the ASL on large-scale climate variations in the Southern Pacific Ocean has not yet been fully established (Fogt et al., 2012; Carrasco, 2021).

Despite their vast territorial extension, the number of climatic records in the sub-Antarctic regions is very low. Most of them are short and inhomogeneous. Therefore, knowledge of climate variability and its connection with the dominant atmospheric patterns remains fragmentary. To counter this deficiency, indirect records of climate variability are used to extend existing instrumental data into the past. Proxy records are useful to provide robust estimates of natural climate variability to determine the extent to which recent changes and trends are anomalous in the context of climate variability over the past centuries or millennia.

Tree-ring records have been used previously to reconstruct past variations in SSA temperature. Boninsegna et al. (1989) developed the first reconstruction of Tierra del Fuego temperature for the interval 1750–1984 using a combination of four *N. pumilio* and *N. betuloides* tree-ring chronologies. The reconstructed summer temperatures (from November to February) show relatively warm periods in the 18th and 19th centuries and gradual warming in the last decades not statistically different from those observed in the past (Boninsegna et al., 1989). Based on seven chronologies of *N. pumilio* tree-ring widths, Aravena et al. (2002) developed a minimum temperature reconstruction for Punta Arenas covering the period 1829–1996. This reconstruction shows that annual minimum temperatures during most of the 19th century remained below average, increased to values close to the long-term mean during 1900–1960, followed by a clear positive trend with above-average temperatures from the 1960s onwards. More recently, Matskovsky et al. (2022) developed a new summer temperature reconstruction (December to February) over the interval 1765–2001 based on a combination of 16 *N. pumilio* and *N. betuloides* chronologies. This new temperature reconstruction indicates a century-long warm period between 1765 and 1905, with brief cold episodes in the 1800s, 1850s-early, 1860s, and 1880s. Although these reconstructions share some tree-ring records, they differ in their assessment of temperature evolution over the last 2.5 centuries (Matskovsky et al., 2022). Part of the differences observed in the reconstructions responds to the different periods (annual vs. summer) used to calibrate temperature variations with tree-ring records, as well as the target variable (minimum vs. mean temperature) of the reconstruction. Another important difference is given by the different spatial distributions of the chronologies used in the reconstructions. Boninsegna et al. (1989) used chronologies of *N. pumilio* and *N. betuloides* from the southeastern (Argentina) sector of Tierra del Fuego, Matskovsky et al. (2022) used records of both species but along the entire southern (Argentina and Chile) sector of the Island, while Aravena et al. (2002) reconstructed the annual minimum temperature of Punta Arenas using only *N. pumilio* records from the entire Chilean region of Magallanes. In addition, the different statistical approaches used to develop the reconstructions may also contribute to the differences between these temperature reconstructions (Matskovsky et al., 2022). These results highlight the need to increase the number and type of proxy records available to obtain more reliable reconstructions of past climate in SSA.

Oxygen isotopes measured in tree ring cellulose ($\delta^{18}O_{TRC}$) have proven to be a powerful tool in paleoclimatology. Records of $\delta^{18}O_{TRC}$ have been successfully used to reconstruct past variations in precipitation (Treydte et al., 2006; Rinne et al., 2013; Foroozan et al., 2020; Wang et al., 2022), air temperature (Porter et al., 2014; Naulier et al., 2015; Lavergne et al., 2016) and drought events (Kress et al., 2010; Xu et al., 2014; Labuhn et al., 2016; Nagavciuc et al., 2019; Zhu et al., 2021). Similarly, $\delta^{18}O_{TRC}$ chronologies have provided valuable information on past variations of large-scale atmospheric circulation (Brienen et al., 2012; Lavergne et al., 2016; Nagavciuc et al., 2019; Pumijumnong et al., 2020; Meier et al., 2020; Balting et al., 2021). In the Southern Hemisphere, monthly and seasonal reconstructions of the AAO have recently been developed based on historical meteorological records (Fogt et al., 2009), tree-ring width chronologies, isotopic variations in Antarctic ice cores, and a combination of these proxies (Villalba et al., 2012; Abram et al., 2014; Dätwyler et al., 2018). In addition, $\delta^{18}O_{TRC}$ of several *Nothofagus* species from SSA have also been used to reconstruct past variations in AAO variability (Meier et al., 2020). Recently, the combined use of $\delta^{18}O_{TRC}$ chronologies of *N. betuloides* and *N. pumilio* from SSA has allowed the development of a reliable reconstruction of the AAO for the last 150 years (Grießinger et al., 2018; Meier et al., 2020). The $\delta^{18}O_{TRC}$ of *N. betuloides* and *N. pumilio* constitute a highly recommended alternative for reconstructing climate variability in the high latitudes of South America (Lavergne et al., 2016; Grießinger et al., 2018; Meier et al., 2020). It is worth mentioning that the dominant *Nothofagus* species in SSA forests can reach ages of >400–500 years

(Llancabure, 2011; Fuentes et al., 2019). Therefore, tree rings of these species provide a unique opportunity to extend the climatic information from instrumental records and characterize their temporal variations in the past centuries.

In this context, the present study examined the climatic information contained in the $\delta^{18}O_{TRC}$ records of *N. pumilio* and *N. betuloides* from different environments in the SSA during the last six decades. The characterization of climate-proxy relationships over the period of instrumental data represents the first step in determining the viability of these isotopic records for reconstructing climate in past centuries. In this paper, we sought to determine the relationships between local climate variability (precipitation, temperature, wind speed, and soil water) and isotopic records derived from *Nothofagus* tree rings. In the second step, we established the relationships between our isotopic records and regional-hemispheric modes of climate variability, such as ASL and AAO. Our study lays the foundation for reconstructing the long-term variability of the dominant forcings of atmospheric circulation in SSA for the last hundred to thousand years.

2. Study site

2.1. Climatic conditions in southernmost South America

Southernmost South America (SSA) includes the southern continental part of Patagonia, Tierra del Fuego, and its adjacent islands (50–56° S; Fig. 1). The Andes Mountains act as an orographic barrier to the humid air masses coming from the Pacific Ocean, inducing precipitation of up to 5000 mm/yr on the western slopes and <200 mm/yr in the eastern sector, only 50–100 km from the Andean peaks (Carrasco et al., 2002; González-Reyes et al., 2017; Viale et al., 2019). The strong precipitation gradient determines the presence of different biotic communities (Pisano, 1977) arranged from hyper-humid Magellanic peatlands and evergreen forests (*N. betuloides*) through mixed (*N. betuloides* and *N. pumilio*) and deciduous (*N. pumilio* and *N. antarctica*) forests to the Magellanic steppe. Our study was conducted in the evergreen *N. betuloides* forest in Navarino Island (NC) and the deciduous *N. pumilio* forest near Punta Arenas (SKI; Fig. 1A and B).

According to instrumental records from Punta Arenas (53° S, 70.8° W, Fig. 1C) and Puerto Williams (54.9° S, 67.6° W, Fig. 1D), the climate of the region is characterized as maritime-cold, with mean summer and winter temperatures of 11 and 2.2 °C in Punta Arenas and 9.6 and 2.3 °C in Puerto Williams, respectively. Precipitation in Punta Arenas (~400 mm/year) is lower than in Navarino Island (~530 mm/year), but the mountainous topography introduces enormous variations in total amounts between relatively close sites. The marked difference in vegetation between the two sites suggests that lower temperatures, particularly in summer, exacerbate differences in precipitation, with wetter forests on Navarino Island than those observed in the forest-steppe ecotone near Punta Arenas. Regional relative humidity in the winter season ranges between 77 and 85%, with an annual average of 72.6%. During the summer, relative humidity is lower (~65%) concurrent with higher temperatures.

2.2. Tree samples

Samples of the two *Nothofagus* species studied were collected during fieldwork in the austral summer of 2020 (Soto-Rogel et al., 2022). The SKI site at 550 m asl near Punta Arenas (53.153° S, 71.042° W) is covered by the deciduous *N. pumilio* forest with a mean height of 10 m. This site has a predominantly SE exposure, an average slope of 25°, and podzolic soils surrounded by alpine meadows. The NC site is located on Navarino Island, separated >300 south of Punta Arenas. This site is dominated by the evergreen *N. betuloides* forest; It is at 350 m asl in the Ukika valley (54.998° S, 67.599° W), and the forest reach an average height of 17 m. The NC site has a western exposure with average slopes of 30–35° and podzolic soils. The NC site combines samples of the NCA and NCB sites in Soto-Rogel et al. (2022).

2.3. α-cellulose extraction

To develop the oxygen isotope chronologies, six individuals of *N. pumilio* from SKI and ten individuals of *N. betuloides* from NC were selected from a total of 26 and 39 trees, respectively (Soto-Rogel et al., 2022). The main analytical criteria for selecting the samples for final $\delta^{18}O_{TRC}$ determination were 1) precise calendar age determination and accurate cross-dating, 2) tree ring width >0.3 mm, otherwise with a wood mass >3.5 mg, and 3) cores with good inter-series correlations.

Annual rings from each sample were cut with a scalpel under a binocular microscope and stored individually. To extract α-cellulose, each sample was treated following the method described by Wieloch et al. (2011). To ensure complete intra-annual homogenization, the final α-cellulose samples were further homogenized using an ultrasound system (Laumer et al., 2009). The homogenized samples were placed in a freeze-drying analyzer for 72 h before isotopic analyses. Finally, ~200 μg of each annual sample were individually packed in silver capsules for final $\delta^{18}O$ determination using an isotope ratio mass spectrometer (Thermo Fisher Delta-V Advantage) coupled to an elemental analyzer (HekaTech). To ensure the reliability of the measurements, $\delta^{18}O$ values were periodically calibrated with laboratory and international standard mean ocean water (SMOW), resulting in an overall analytical precision of >0.2‰.

2.4. Characteristics and evaluation of $\delta^{18}O_{TRC}$-climate

The consistency of the $\delta^{18}O_{TRC}$ chronologies was assessed by calculating the mean correlation between all individual series (Rbar, Cook and Briffa, 1990) and the expressed population signal (EPS, Wigley et al., 1984). Both statistics assess how well the individual oxygen isotope time series represent a theoretically infinitely replicated population. At each site, individual records were averaged to obtain the final $\delta^{18}O_{TRC}$ chronology. The first-order autocorrelations for the SKI and NC isotope records are −0.009 and 0.027, respectively. We calculated Pearson correlation coefficients between our isotopic chronologies and monthly or seasonal climate records to analyze species-specific responses to climate. The climatic parameters used to assess proxy-climate relationships were precipitation (PREC), maximum and minimum temperature (TMAX and TMIN, respectively), wind speed (WS), relative humidity (RH), soil water (SW) and mean sea level pressure (MSL, Table 1). Climate data from Punta Arenas (53.00° S, 70.83° W) and Puerto Williams (54.93° S, 67.61° W), located 20 km and 8 km from SKI and NC, respectively, were used for comparisons. In addition to the station datasets (Table 1), we used monthly climate data from the ERA5 (Hersbach et al., 2020; Bell et al., 2021) and ERA5-Land (Muñoz-Sabater et al., 2021) reanalyses with specific grids for SKI (53.15°S, 70.04°W) and NC (54.99°S, 67.59°W). Beck et al. (2021) noted that soil moisture information from the ERA5-Land model performs relatively well for regions in North America, Europe, Africa, and Australia. The ERA5-land soil moisture data quality has not been explicitly tested in South America. However, due to the lack of other reliable datasets with similar spatial resolution, we decided to use the ERA5-Land model dataset in our study.

The climate imprints of different regional and hemispheric indices were investigated to study the influences of large-scale atmospheric circulation modes on the $\delta^{18}O_{TRC}$ chronologies (Table 2). The Amundsen Sea Low central pressure index is calculated from reanalysis data for an area west of the Antarctic Peninsula (60–80° S, 170–298° E). It starts in the year 1979 (ASL, Hosking et al., 2013). The AAO-CPC index is based on CPC reanalysis pressure fields at the 700 mb height from 20°S to the south pole and starts in 1979 (Cpc, 2022). The AAO-Marshall index is based on pressure data from meteorological stations located around 40° S and 60° S and is available since 1957 (Marshall, 2003). The AAO-NCEP-NCAR is an index based on sea level pressure differences

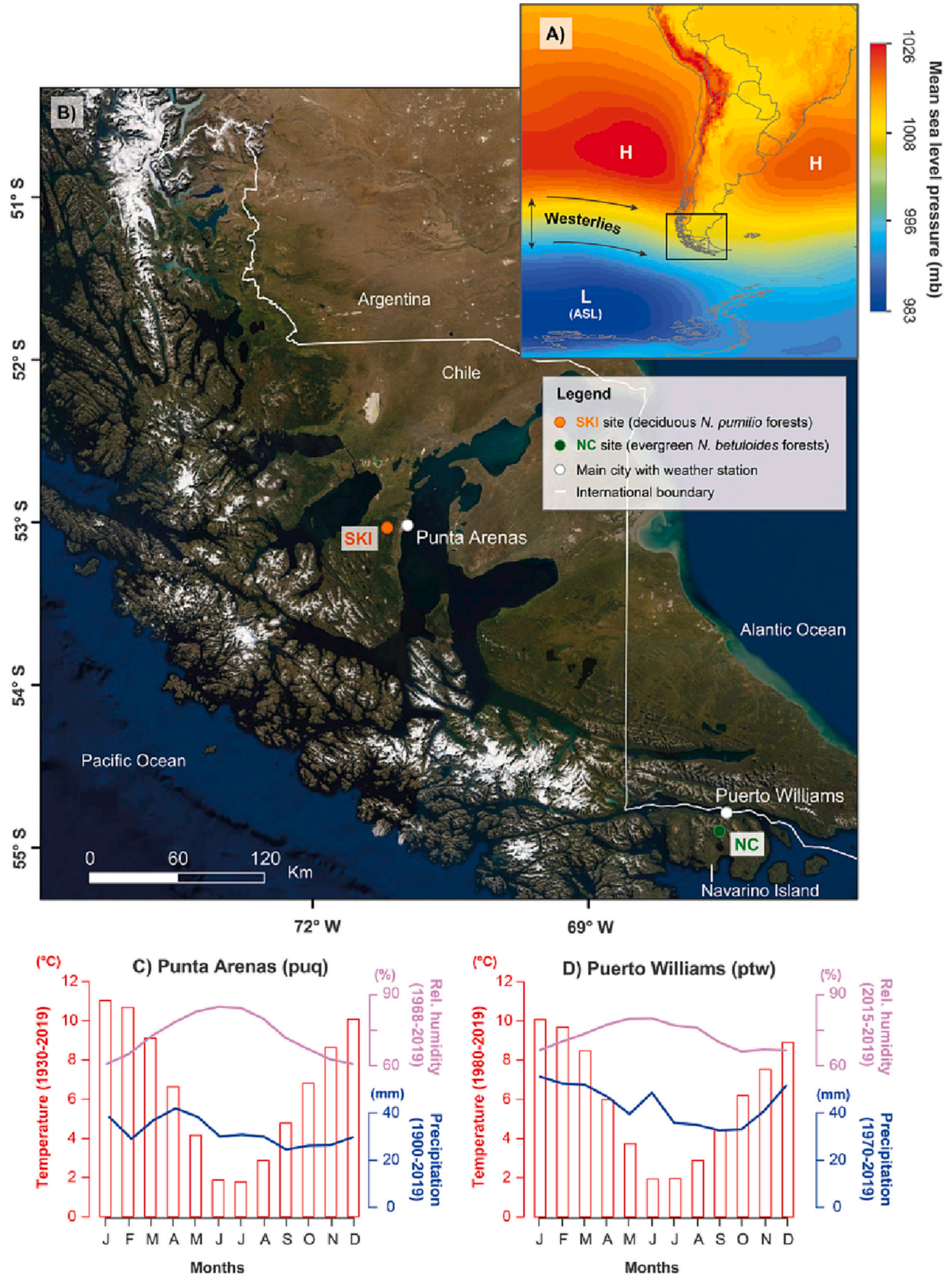

Fig. 1. A) Mean sea-level pressure during spring-summer (September to February; Hersbach et al., 2020) over the South America-Antarctic Peninsula sector in the Southern Hemisphere. The locations of the mid-latitude high (H) and low (L) pressure centers and westerly winds are indicated (in black). The position of the Amundsen Sea Low (ASL) is also indicated. The black box in A corresponds to the study area in B. Orange, and green circles show the location of the $\delta^{18}O_{TRC}$ chronologies of *N. pumilio* and *N. betuloides*, respectively. The climate diagram includes data from C) Punta Arenas (puq) and D) Puerto Williams (ptw) weather stations. (For interpretation of the references to color in this figure legend, the reader is referred to the web version of this article.)

Table 1
Geographical location of the meteorological stations and the ERA5 and ERA5-land grids used in this study. Climatic variables and periods are also indicated.

Meteorological Station	Lat (S) Long (W)	Variable	Period	Source
Punta Arenas (puq)	53.00 70.83	MSL: mean sea level pressures (mb)	1968–2021	(Dmc, 2022)
		PREC: precipitation (mm)	1900–2021	
		RH: relative humidity (%)	1967–2021	
		TMAX: maximum temperature (°C)	1930–2021	
		TMIN: minimum temperature (°C)	1930–2021	
		WS: wind speed (km/h)	1967–2021	
Puerto Williams (ptw)	54.93 67.61	MSL: mean sea level pressures (mb)	1969–2021	(Dmc, 2022)
		PREC: precipitation (mm)	1970–2021	
		TMAX: maximum temperature (° C)	1980–2021	
		TMIN: minimum temperature (°C)	1980–2021	
		WS: wind speed (km/h)	1986–2021	
ERA5	ski (53.15, 71.04) nc (54.99, 67.59)	MSL: mean sea level pressures (Pa)	1950–2021	(Hersbach et al., 2020; Bell et al., 2021)
		PREC: total precipitation (m)		
		RH: relative humidity at 1000 hPa (%)		
		2mT: temperature at 2 m(K)		
		WS: wind speed at 10 m (m/s)		
ERA5-Land	ski (53.15, 71.04) nc (54.99, 67.59)	SW L1: Soil water layer 1 (0–7 cm, m^3/m^3)	1950–2021	(Muñoz-Sabater et al., 2021)
		SW L2: Soil water layer 2 (7–28 cm, m^3/m^3)		
		SW L3: Soil water layer 3 (28–100 cm, m^3/m^3)		
		SW L4: Soil water layer 4 (100–280 cm, m^3/m^3)		

(NCEP-NCAR) between 40° and 65° S and starts in 1948 (Knmi, 2022).

In addition, we calculated spatial correlation patterns between our $\delta^{18}O_{TRC}$ chronologies and climate fields from the ERA5 reanalysis (Hersbach et al., 2020). The climate variables used for comparisons were mean sea level pressure (MSL), wind speed (WS), precipitation (PREC), and maximum and minimum temperature (TMAX and TMIN) over the period 1960–2021 using the KNMI Climate Explorer (Trouet and van Oldenborgh, 2013; Knmi, 2022).

3. Results

3.1. Characteristics of the $\delta^{18}O_{TRC}$ chronologies

Regional $\delta^{18}O_{TRC}$ records from the deciduous *N. pumilio* forest near Punta Arenas (SKI-$\delta^{18}O_{TRC}$) and the evergreen *N. betuloides* forest on Navarino Island (NC-$\delta^{18}O_{TRC}$) cover the period 1960 to 2019 (Fig. 2), with inter-series correlations (RBar) of $r = 0.62$ and $r = 0.73$, respectively. The isotopic variations of the SKI-$\delta^{18}O_{TRC}$ series range between 25 and 30‰ (mean 27.09‰) and show no clear trend (Fig. 2A). In contrast, the NC-$\delta^{18}O_{TRC}$ series showed more significant variability ranging between 27 and 33‰ (mean 29.18‰) and a significant positive trend ($p < 0.01$; Fig. 2B). EPS values ranged from 0.90 (SKI) to 0.97 (NC). Both statistics indicate good quality of the chronologies and adequate representation of the common signal in their respective populations (Cook and Briffa, 1990).

3.2. Climate-$\delta^{18}O_{TRC}$ relationships

Fig. 3A shows correlation coefficients between $\delta^{18}O_{TRC}$ records and several climatic variables, including precipitation, maximum temperature, wind speed, and soil water content (estimated at different L1 and L2 depths). The chronologies for both species show negative relationships with precipitation and soil water content (at both L1 and L2) for the spring-summer months and positive relationships with maximum temperature and wind speed throughout the year. Significant positive correlations were also observed between NC and soil water during August and September (late austral winter and early spring). The most significant correlations occurred during the austral months of late winter-spring-summer (August to February) for NC and late spring-summer (November to February) for SKI. For the NC-$\delta^{18}O_{TRC}$ record, the highest relationships occurred with soil water content at L2 (7–28 cm; Fig. 3E, October to February), $r = -0.76^{**}$, $r^2 = 0.58$), followed by ERA5 wind speed (Fig. 3D, November to February, $r = 0.69^{**}$, $r^2 = 0.48$), precipitation (Fig. 3B, November to January, $r = -0.66^{**}$, $r^2 = 0.44$) and maximum temperature (Fig. 3C, October to December, $r = 0.62^{**}$, $r^2 = 0.38$). The SKI-$\delta^{18}O_{TRC}$ record was highly related to January (summer month) soil water content in the L2 layer (Fig. S1, January, $r = -0.60^{**}$, $r^2 = 0.36$), ERA summer precipitation (Fig. S1, November to January, $r = -0.56^{**}$), and to a lesser degree to maximum temperature conditions during the austral summer (December to February, $r = 0.32^{*}$). No significant relationships were observed between SKI-$\delta^{18}O_{TRC}$ and wind speed (February, $r = 0.25$).

Following the climate-$\delta^{18}O_{TRC}$ relationships illustrated in Fig. 3, spatial patterns were estimated between the different climate variables from the ERA5 reanalysis and the isotopic records during the austral spring-summer season (October to February) for NC-$\delta^{18}O_{TRC}$ and during the austral summer (December to February) for SKI-$\delta^{18}O_{TRC}$ (Fig. 4). The NC-$\delta^{18}O_{TRC}$ chronology showed a close annular pattern with strong significant positive and negative relationships with sea level pressure at mid-latitudes and over Antarctica, respectively, resembling the sea level pressure pattern associated with the AAO in the Southern Hemisphere (MSL, Fig. 4A). A strong positive correlation pattern with wind speed (WS, Fig. 4B) was also observed throughout the Southern Ocean (somewhat similar to that recorded for precipitation, not shown). On the

Table 2
Southern Hemisphere regional and hemispheric circulation indices/modes used to assess proxy-climate relationships.

Index	Methodology	Period	Source
Amundsen Sea Low (ASL)	Sea level pressures from NCEP reanalysis	1979–2021	(Hosking et al., 2013) http://scotthosking.com/asl_index
CPC's Antarctic Oscillation (AAO-CPC)	Atmospheric pressures at 700 mb from reanalysis	1979–2021	(Cpc, 2022)
Marshall's Antarctic Oscillation (AAO-Marshal)	Sea level pressures from weather stations	1957–2021	(Marshall, 2003)
NCEP/NCAR's Antarctic Oscillation (AAO-NCEPNCAR)	Sea level pressures from NCEP/NCAR	1948–2021	(Knmi, 2022)

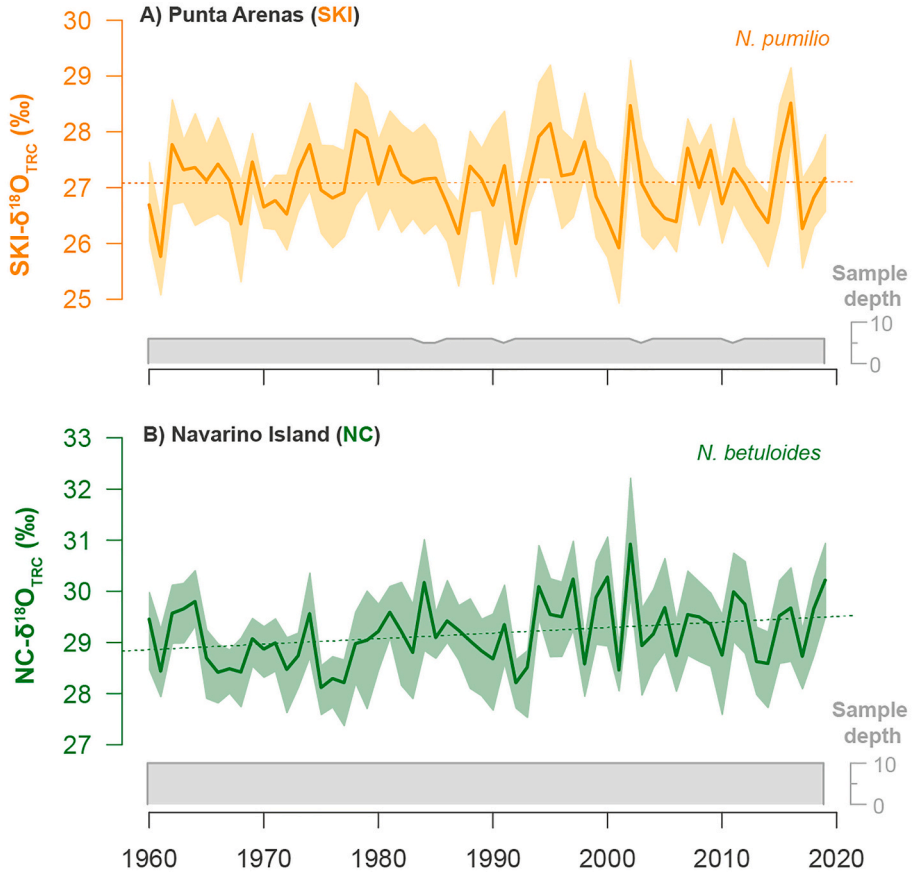

Fig. 2. Inter-annual records of $\delta^{18}O_{TRC}$ (‰) in *Nothofagus* forests from SSA. A) The deciduous *N. pumilio* forest at the SKI site near Punta Arenas, and B) the evergreen *N. betuloides* forest at the NC site on Navarino Island. Dark lines indicate mean annual $\delta^{18}O_{TRC}$ values, and the shaded area represents the 95th and 5th percentiles. Dotted lines indicate linear trends (linear regression) of isotopic records.

other hand, the SKI-$\delta^{18}O_{TRC}$ series displayed similar but weaker spatial correlation patterns than those observed with the NC-$\delta^{18}O_{TRC}$ record. The SKI-$\delta^{18}O_{TRC}$ showed patterns of significant positive correlation with sea level pressure at mid-latitudes in the vicinity of South America, Africa, New Zealand, the Indian Ocean, and a center of negative correlation over the Antarctic continent (Fig. 4C). Significant correlation patterns with wind speed are spatially limited to a small sector of the Southern Ocean off the west coast of the Antarctic Peninsula (Fig. 4D).

3.3. Atmospheric circulation-$\delta^{18}O_{TRC}$ relationships

Our $\delta^{18}O_{TRC}$ chronologies also showed strong relationships with regional (ASL) and large-scale (AAO) atmospheric circulation modes in the Southern Hemisphere (Fig. 5A). While the most significant relationships with NC occurred during the austral spring-summer months, for SKI, they were limited to the austral summer. Highly significant relationships were observed between NC-$\delta^{18}O_{TRC}$ chronology and the ASL index from mid-spring to early austral summer (Fig. 5B, October to January, $r = -0.80^{**}$, $r^2 = 0.64$), consistent with highly significant correlations with Southern Hemisphere AAO indices for the same season; for example for AAO-CPC (Fig. 5C, October to January, $r = 0.77^{**}$, $r^2 = 0.59$), AAO-Marshall (Fig. 5D, October to February, $r = 0.69^{**}$, $r^2 = 0.48$) and AAO-NCEPNCAR (Fig. 5E, October to January, $r = 0.69^{**}$, $r^2 = 0.48$). In contrast, the SKI-$\delta^{18}O_{TRC}$ chronology exhibited comparatively weaker relationships with circulation modes, although significant relationships occurred during the austral summer for all indices, e.g., AAO-CPC (Fig. S1, December to February, $r = 0.47^{**}$), AAO-Marshall (December to February, $r = 0.35^{**}$), AAO-NCEPNCAR (December to February, $r = 0.31^{**}$), ASL (Fig. S1, December to February, $r = -0.44^{**}$).

To evaluate the consistency between our isotopic records and other proxies associated with AAO variations, we compare the temporal variation of the NC-$\delta^{18}O_{TRC}$ record with currently available AAO reconstructions (Fig. 6). Numerous above-average isotopic events in the NC-$\delta^{18}O_{TRC}$ are associated with predominantly positive AAO indices. The first austral summer AAO reconstruction was based solely on ring-width chronologies from South America and New Zealand (Villalba et al., 2012). Most tree-ring chronologies were located at mid-latitudes in the Southern Hemisphere, including *Austrocedrus chilensis* (37° S to 43° S) and *Araucaria Araucana* (38 to 40° S) in South America and *Halocarpus biformis* (42° to 45° S) in New Zealand. Over the common interval 1960–2006, the AAO reconstruction and our $\delta^{18}O_{TRC}$ record are significantly correlated ($r = 0.38^{**}$). Abram et al. (2014) provided the first-millennium annual AAO reconstruction based on a larger proxy dataset, including tree-ring records at mid-latitudes from South America and high-latitude δ^2H in ice cores from the Antarctic Peninsula and Antarctic continental regions. These AAO reconstructions show the strongest relationships with the NC isotopic record (Fig. 6, $r = 0.43^{**}$). Dätwyler et al. (2018) recently developed austral summer (DJF) and annual AAO reconstructions using four different methodological approaches. The summer AAO reconstruction, including nine Australasian and South American tree-ring records, six Antarctic ice core records, four Australasian coral records, and one South American documentary record, significantly correlates to our NC isotopic series ($r = 0.41^{**}$). In addition to these proxy-based AAO reconstructions, Fogt et al. (2009) used the longest instrumental sea-level pressure records in the Southern Hemisphere to extend the AAO series to the mid-nineteen century (Fig. 6, $r = 0.43^{**}$).

In a recent contribution, Meier et al. (2020) provide the first AAO

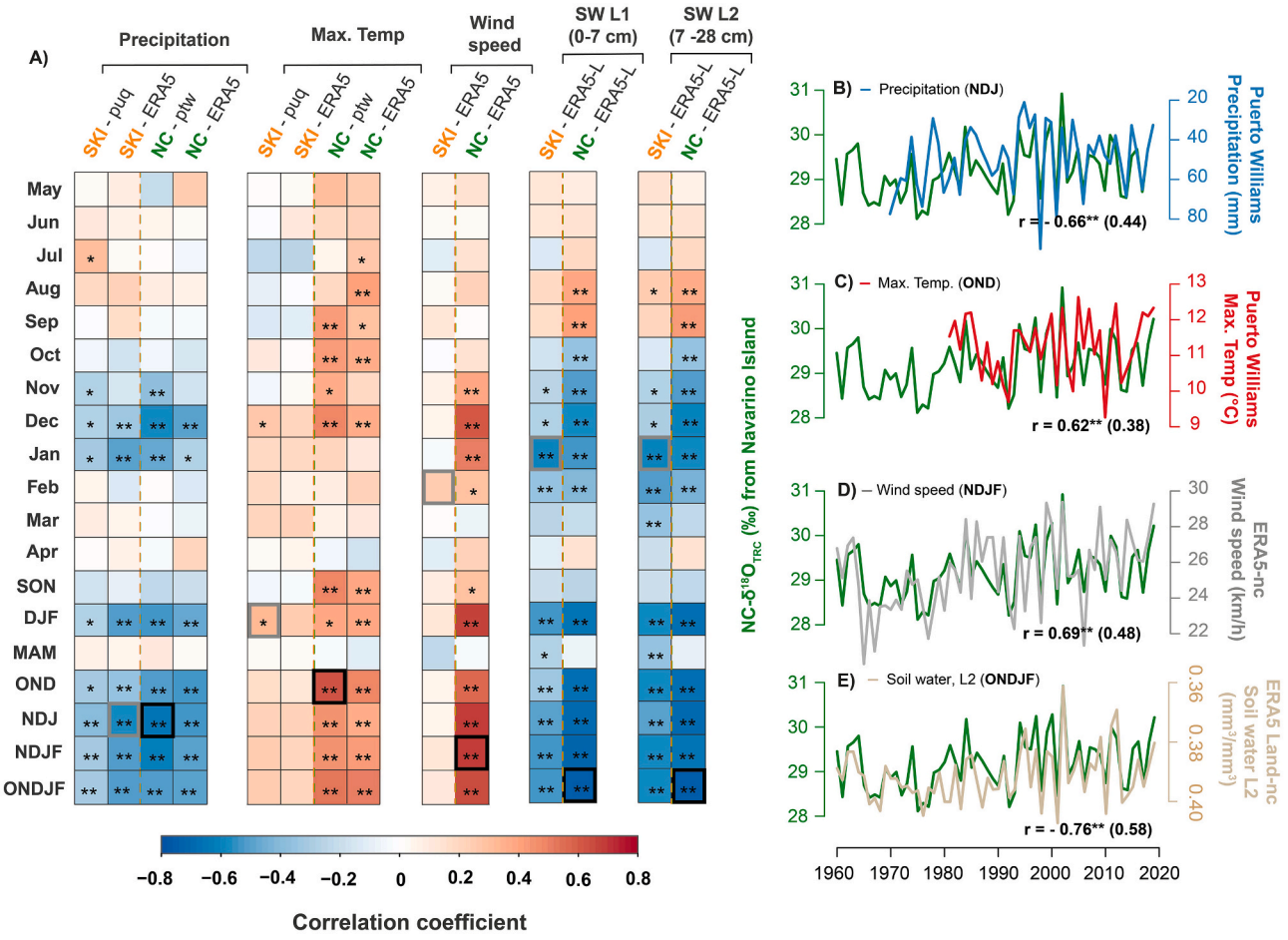

Fig. 3. A) Relationships between $\delta^{18}O_{TRC}$ chronologies of *N. pumilio* (SKI, orange color) and *N. betuloides* (NC, green color) with precipitation and maximum temperature at Punta Arenas (puq) and Puerto Williams (ptw), respectively, and the ERA5 reanalysis. Wind speed and soil water content (SW) at L1 (0–7 cm) and L2 (7–28 cm) were taken from the ERA5 reanalysis. Correlations are presented for 12 months, from the previous May to the current April, and for different seasons (spring, SON: September to November, summer, DJF: December to February, autumn, MAM: March to May, late spring, OND: October to December, early summer, NDJ: November to January, long summer, NDJF: November to February and late spring-early summer ONDJF: October to February). Significant correlations are indicated: $p < 0.05$ (*) and $p < 0.01$ (**). The most significant relationships between climate at Puerto Williams (ptw) and NC-$\delta^{18}O_{TRC}$, highlighted in black-bordered boxes in A, are shown in the right panels for B) precipitation, C) maximum temperature, D) wind speed, and E) soil water. Correlation coefficients (r) and explained variance (r^2 in parentheses) are indicated in each panel. Gray bordered boxes in A indicate the most significant relationships between Punta Arenas climate (puq) and SKI-$\delta^{18}O_{TRC}$. (For interpretation of the references to color in this figure legend, the reader is referred to the web version of this article.)

reconstruction based on $\delta^{18}O_{TRC}$ records from multi-*Nothofagus* species from southern South America (Fig. 6B). A stable oxygen isotope time series from *Nothofagus betuloides* was developed at the Schiaparelli Glacier (54.4° S) within the hyper-humid Austral Andes. This isotopic record was merged with a $\delta^{18}O_{TRC}$-*Nothofagus pumilio* chronology from the Perito Moreno Glacier (50° S) (Grießinger et al., 2018) to developed an AAO reconstruction for the last 150 years. This reconstruction explains 62% of the September–February AAO variations and shows an increasing trend towards more positive index values during recent decades (Meier et al., 2020).

4. Discussion

This study contributes two new annually-resolved $\delta^{18}O_{TRC}$ chronologies from *Nothofagus* forests in southernmost South America (SSA). The SKI-$\delta^{18}O_{TRC}$ record from deciduous *N. pumilio* forests in the steppe-forest ecotone at Punta Arenas is the most southeastern isotopic site for this species. In contrast, the NC-$\delta^{18}O_{TRC}$ chronology from evergreen *N. betuloides* forests on Navarino Island is the southernmost tree-ring-based record worldwide. Both chronologies represent robust isotopic records with considerable replicate common signal (EPS > 0.90).

At our study sites, $\delta^{18}O_{TRC}$ values generally increase with low soil water availability, mostly concurrent with strong wind speeds and high temperatures (Fig. 3 and Fig. S1). Such climatic conditions are associated with the positive phase of AAO and low pressures in the ASL sector (Fig. 5). In contrast, lower $\delta^{18}O_{TRC}$ values are related to high soil moisture levels, the negative phase of AAO, and low ASL index values (Fig. 3, Fig. 5, and Fig. S1). This association suggests that supra-regional atmospheric circulation modes (AAO and ASL) and their associated climatic conditions are the main drivers of $\delta^{18}O_{TRC}$ variations in SSA. In addition, our study shows that droughts and wind speed promote ^{18}O isotopic enrichment in SSA tree rings, results in agreement with models of ^{18}O isotopic fractionation in tree rings (Barbour et al., 2002; Gessler et al., 2013, 2014; Roden et al., 2000), and consistent with previous studies of $\delta^{18}O_{TRC}$ in SSA (Tognetti et al., 2014; Lavergne et al., 2016; Grießinger et al., 2018; Meier et al., 2020).

Positive relationships of $\delta^{18}O_{TRC}$ in *Nothofagus* forests with temperature and negative with precipitation have also been reported for South America by Lavergne et al. (2016), Grießinger et al., 2018, and Meier et al. (2020). Similarly, the strong AAO signal detected in our NC-$\delta^{18}O_{TRC}$ chronology is in good agreement with previous studies on the spatially consistent influence of AAO on tree $\delta^{18}O_{TRC}$ variations in SSA (Grießinger et al., 2018; Meier et al., 2020). Our results also provide the basis to support, for the first time, strong relationships between stable

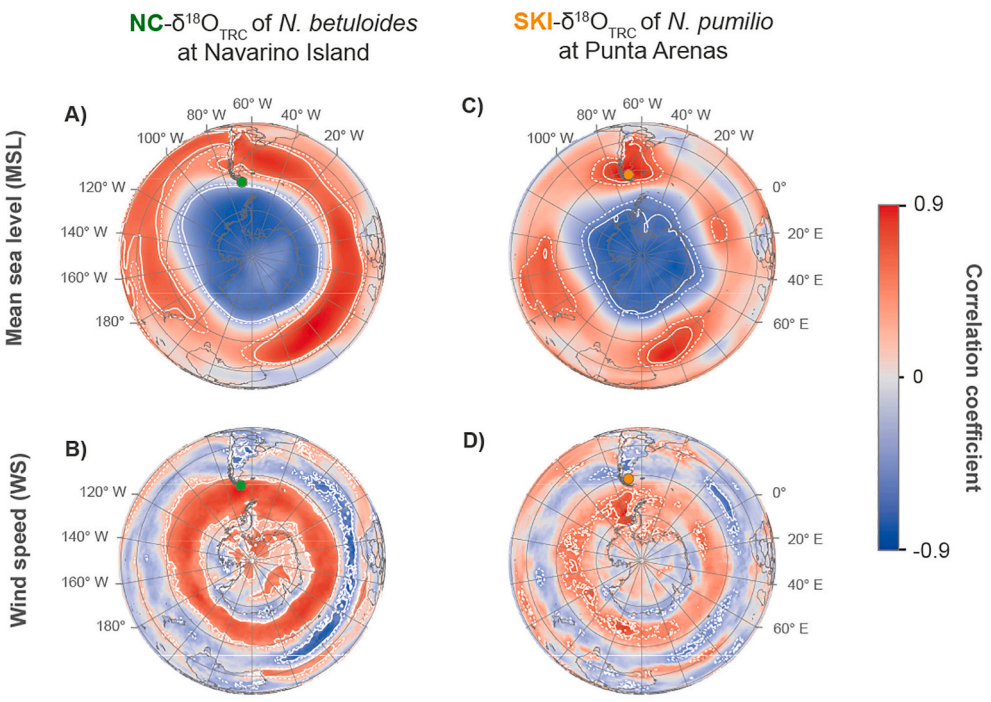

Fig. 4. Spatial correlation patterns between the ERA5 reanalysis and the two $\delta^{18}O_{TRC}$ chronologies (NC and SKI). The first column shows the spatial correlations between NC-$\delta^{18}O_{TRC}$ (green circle: A and B) and ERA5 mean sea level pressure and wind speed during the austral spring-summer (October to February). The second column shows the spatial correlations between SKI-$\delta^{18}O_{TRC}$ (orange circle: C and D) and ERA5 mean sea-level pressure and wind speed during the austral summer (December to February). Dashed and solid white lines indicate significant correlations at the $p < 0.05$ and $p < 0.01$, respectively. (For interpretation of the references to color in this figure legend, the reader is referred to the web version of this article.)

isotopes in *Nothofagus* forests and soil water content at different depths. The $\delta^{18}O_{TRC}$ in SKI and NC was strongly negatively related to soil water dynamics at depths between 0 and 7 cm and 7–28 cm (L1 and L2 levels, respectively). Consistent with these results, Soto-Rogel et al. (2022) reported significant positive relationships between *N. betuloides* ring width on Navarino Island and precipitation during the spring-summer months (September to February). These observations would indicate that the isotopic composition of soil water is an important factor regulating the $\delta^{18}O$ signal in *N. betuloides* rings.

We also report the novelty of strong positive correlations between the NC-$\delta^{18}O_{TRC}$ chronology and wind speed. Previously, Soto-Rogel et al. (2022) reported negative correlations between wind speed and the *N. betuloides* ring width on Navarino Island. The NC site is directly exposed to strong southwesterly winds from the Southern Ocean. Meier et al. (2020) indicated that a higher proportion of heavy ^{18}O isotopes in the *N. betuloides* forest near the Schiaparelli glacier would be due to increased evaporation, which could be induced by the prevailing high wind speeds during the austral summer. Also, strong wind speeds negatively affect photosynthesis through reduced stomatal conductance (Smith and Ennos, 2003; Iogna et al., 2013).

In this contribution, we also document differences in the sensitivity of $\delta^{18}O_{TRC}$ records to climatic variations. Variations of NC-$\delta^{18}O_{TRC}$ in the evergreen *N. betuloides* forest on Navarino Island are strongly dependent on variations in local climate parameters (precipitation, maximum temperature, wind speed, soil water at different depths, Fig. 3) and atmospheric forcings (AAO and ASL, Fig. 5) that induce these variations. In contrast, the SKI-$\delta^{18}O_{TRC}$ record of deciduous *N. pumilio* at Punta Arenas showed weaker relationships with the local climate. While the SKI-$\delta^{18}O_{TRC}$ record provides some potential as a proxy for precipitation and soil water dynamics during summer, isotopic variations in evergreen *N. betuloides* are more strongly related to climatic variations over a more extended period in the growing season (austral spring-summer, Fig. 3). While SKI showed comparatively limited spatial correlation during summer, NC spatial patterns showed greater spatial representativeness with stronger relationships during the spring and summer seasons. These differences in isotopic response could be explained by species- and site-specific characteristics. Previous studies report that differences in responses to climate among species of the genus *Nothofagus* are related to different physiological strategies of adaptation to drought (Bucci et al., 2012; Soliani et al., 2021). Deciduous *Nothofagus*, such as *N. pumilio*, exhibit anisohydric behavior, keeping their stomata open for CO_2 uptake under water stress conditions and, consequently, continue to lose water by transpiration (Bahamonde et al., 2019; Varela et al., 2010). In contrast, in evergreen *Nothofagus*, the coordination of different stress strategies, either within leaves or between leaves and conducting tissue in trunks and branches, allows evergreen species to optimize carbon assimilation during dry periods (Bucci et al., 2019). Although there are no specific studies on the response of *N. betuloides* to water deficit, Bucci et al. (2019) indicate that evergreen *Nothofagus* species (such as *N. dombeyi*) are more resistant to drought, with a capacity comparable to xeric tree species of the Andean-Patagonian forest such as *Austrocedrus chilensis* and *Maytenus boaria*.

Site conditions could also be another factor associated with differences in $\delta^{18}O_{TRC}$ responses to climate. Csank et al. (2016) recorded significant differences in $\delta^{18}O_{TRC}$ between sites, while Marshall and Monserud (2006) observed that differences in $\delta^{18}O_{TRC}$ between individual trees were more significant than between species. In southern Patagonia, *N. betuloides* trees exposed to high water stress induced by warmer and drier summers show marked reductions in tree growth induced by a decrease in stomatal conductance (Soto-Rogel et al., 2022). Srur et al. (2008) observed that radial growth of *Nothofagus pumilio* in mesic forests of the southern Patagonian Andes benefits from wet and relatively cold conditions. These authors observed that in drier sites, the photosynthetic rate is severely limited by water deficits, so the reduction in radial growth is not compensated by increased water use efficiency. We hypothesize that *N. betuloides* at the NC site uses mainly meteoric water and thus maintains a high relationship with the local climate parameters, connected with regional (ASL) and hemispheric (AAO) modes of circulation. In contrast, *N. pumilio* from SKI would use a mixture of groundwater and meteoric water, so the ^{18}O climate signal is weaker than the NC site. These differences reinforce the importance of attending to the analysis of stable isotope composition ($\delta^{13}C_{TRC}$ and $\delta^{18}O_{TRC}$) to the topographic and hydrological conditions of the sampling sites (Belmecheri et al., 2022). However, we do not rule out that species differences and site conditions interact with each other to modulate stable isotope-climate relationships.

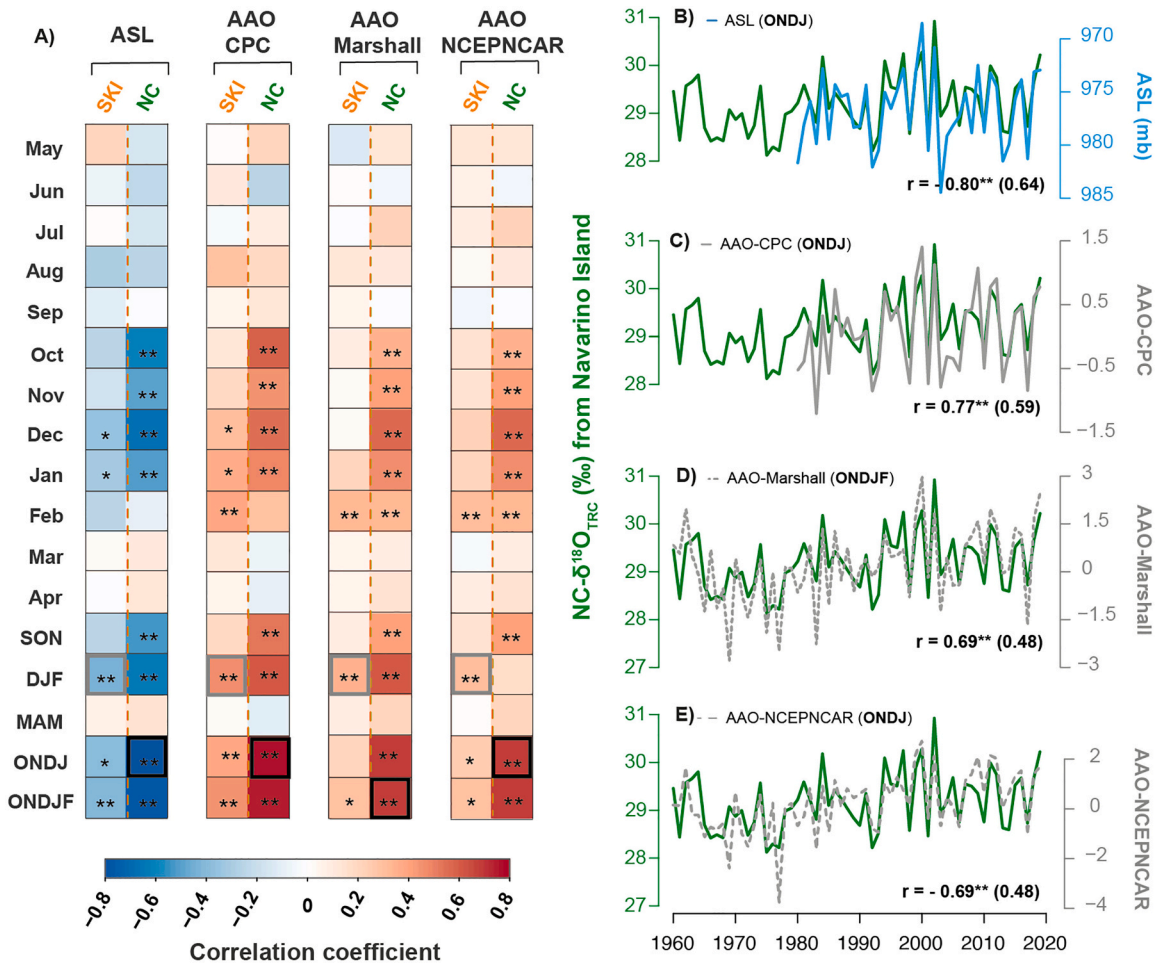

Fig. 5. A) Relationships between Southern Hemisphere (SH) atmospheric circulation indices (AAO-CPC, AAO-Marshall, AAO-NCEPNCAR, and ASL) and $\delta^{18}O_{TRC}$ chronologies (SKI, orange color; NC, green color). Correlations are presented for 12 consecutive months from May to April, and different seasonal means (SON: September to November, DJF: December to February, MAM: March to May, ONDJ: October to January, and ONDJF: October to February). Significant correlations are indicated: $p < 0.05$ (*) and $p < 0.01$ (**). The most significant relationships between SH circulation indices and the NC-$\delta^{18}O_{TRC}$, highlighted in black-bordered boxes in A, are shown in the right panels for B) ASL, C) AAO-CPC, D) AAO-Marshall, and E) AAO-NCEPNCAR. Correlation coefficients (r) and explained variance (r^2 in parentheses) are indicated in each panel. Boxes with gray borders in A indicate the most significant relationships between SH and SKI-$\delta^{18}O_{TRC}$ circulation indices. (For interpretation of the references to color in this figure legend, the reader is referred to the web version of this article.)

Our NC-$\delta^{18}O_{TRC}$ chronology of the evergreen *N. betuloides* forest in Navarino Island was able to reproduce with high fidelity the interannual variations of the local climate parameters and atmospheric circulation indices such as the Amundsen Sea Low (ASL) and Antarctic Oscillation (AAO) during the spring-summer season. The ASL index has been proposed to measure the large-scale interannual sea level pressure in the southeastern Pacific Ocean (Hosking et al., 2013). The potential temporal extension of our tree-ring-based isotopic record on Navarino Island over the last 400–500 years would offer the unique opportunity to characterize the evolution of sea-level pressure variations in this sector of the South Pacific under different global thermal conditions, such as the Little Ice Age and the current global warming. This information is highly relevant for assessing the ability of climate models to reproduce interannual to multi-decadal climate changes in this sector of the South Pacific Ocean, which exhibits high atmospheric variability (Garreaud et al., 2021).

ASL variations have also been related to other atmospheric circulation indices such as the AAO and SOI (Southern Oscillation; Fogt et al., 2012). Low ASL pressure values coincide with positive AAO anomalies and La Niña events (positive SOI; Turner et al., 2013). Long-term reconstructions of the ASL would allow assessing the stability in climate teleconnections between the ASL and both tropical and high-latitude atmospheric forcings. Depending on the intensity of the forcing anomalies and their tropical-extratropical interactions, climate events of different magnitudes will impact the SSA local climate (Garreaud, 2018).

Although past AAO variations have previously been reconstructed using $\delta^{18}O_{TRC}$ from a combination of two *Nothofagus* species (Meier et al., 2020) or multiple proxy records, including $\delta^{2}H$ variations in ice cores (Abram et al., 2014), our work is the first to demonstrate the high potential of *Nothofagus betuloides* to provide robust AAO reconstructions based solely on interannual variations of $\delta^{18}O_{TRC}$ in the annual rings of this species. Given the considerable longevity of *N. betuloides* (Llancabure, 2011; Fuentes et al., 2019), annual variations of $\delta^{18}O_{TRC}$ of *N. betuloides* provide excellent material to reconstruct the dominant oscillatory modes of climate variability at high SH latitudes over the last 400 years.

5. Conclusions

Two 60-year $\delta^{18}O_{TRC}$ chronologies from the evergreen *N. betuloides* and deciduous *N. pumilio* have been developed to determine their relationships with local and large-scale circulation modes in the Southern Hemisphere. According to our analyses, the new chronologies capture a large percentage of the total spring-summer variations in temperature, precipitation, and wind speed, which modulate other site conditions

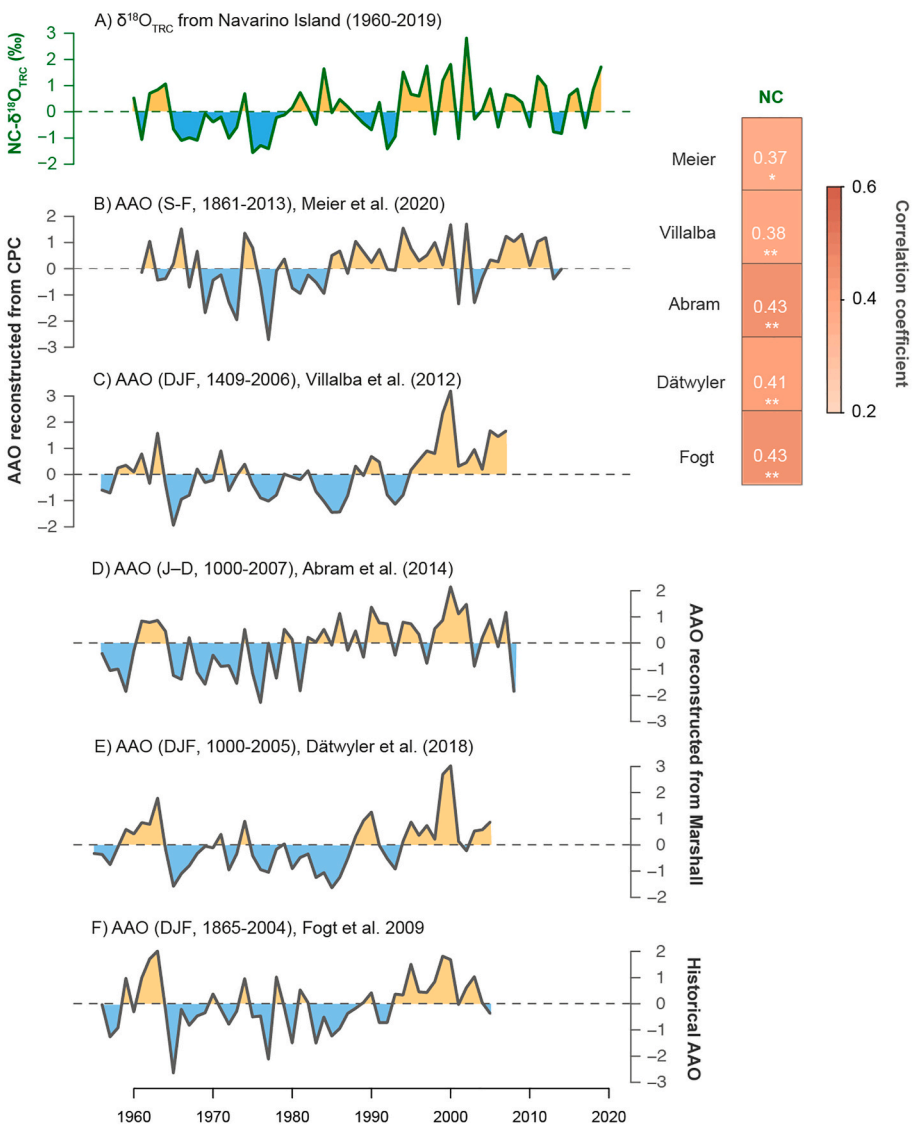

Fig. 6. *Z*-score comparison between A) the $\delta^{18}O_{TRC}$ chronology of Navarino Island (NC) and available AAO reconstructions: B) Spring-summer (1861–2013) AAO reconstruction from Meier et al. (2020) based on $\delta^{18}O$ of *N. betuloides* and *N. pumilio* forests from the Schiaparelli and Perito Moreno glaciers, respectively. C) Summer AAO reconstruction (1409–2006) from Villalba et al. (2012) based on ring widths of different tree species in the Southern Hemisphere. D) Annual reconstruction (1000–2007 AP) of Abram et al. (2014) based largely on $\delta^{2}H$ of the Antarctic ice core. E) Summer reconstruction (1000–2005 AP) by Dätwyler et al. (2018) based on multiple proxies, and F) Historical summer reconstruction (1865–2004 AP) by Fogt et al. (2009) based on long-term records from Southern Hemisphere weather stations. Z-score correlation coefficients (r) were calculated over the common period 1960–2004 between our NC-$\delta^{18}O_{TRC}$ record and available AAO reconstructions.

such as local soil water content. On regional to hemispheric scales, isotopic chronologies are strongly related to ASL and AAO atmospheric circulation modes. We observed that interannual variations in the $\delta^{18}O_{TRC}$ chronology of the evergreen *N. betuloides* show more robust relationships with climate during a longer spring-summer growing season (October to February) than those observed for the deciduous species. The $\delta^{18}O_{TRC}$ record of *N. pumilio* is significantly, but weaker, related to summer climatic conditions (December to February). We assume that differences in climatic sensitivity among species reflect species-specific characteristics and specificities of site conditions. In our study, the higher groundwater use by the deciduous *N. pumilio* could mask the relationships between $\delta^{18}O$ and climate. Consequently, species and site attributes may induce differences in the climatic sensitivity of isotopic records.

Our results show that the isotopic composition of the evergreen *N. betuloides* forest on Navarino Island represents a valuable proxy for reconstructing climate in southern South America and the Southern Hemisphere for the last 4–5 centuries (Llancabure, 2011; Fuentes et al., 2019). However, further research is needed to unravel differences in the climatic sensitivity of deciduous *N. pumilio* and evergreen *N. betuloides* forests, as well as to examine the full potential of both tree-ring isotopic records for climate reconstructions.

In comparison to other regions, particularly in the Northern Hemisphere, the number of stable isotope records in SSA is reduced, suggesting the need to develop additional $\delta^{18}O_{TRC}$ records to validate our results and provide a geographically extended network of sites that would warranty solid reconstructions of past climate variability at different spatial scales in SSA. In addition, it is necessary to complement our study with stable carbon isotopes ($\delta^{13}C_{TRC}$) to model soil-plant-atmosphere relationships, which may provide information on the ecophysiological strategies of SSA forests under recent and future climate changes.

Funding

This work was supported by the ANID-Chilean scholarship (grant 72190234) and by the ANID-BMBF project AVOID (grant no. 180005 and FKZ 01DN19036). J.C.A. acknowledges Fondecyt (grant 1180717) and ANID/BASAL FB210018.

CRediT authorship contribution statement

Pamela Soto-Rogel: Conceptualization, Methodology, Formal analysis, Writing – original draft, Writing – review & editing. **Juan Carlos Aravena:** Conceptualization, Writing – original draft, Writing – review & editing. **Ricardo Villalba:** Conceptualization, Writing –

original draft, Writing – review & editing. **Wolfgang Jens-Henrik Meier:** Methodology, Writing – review & editing. **Jussi Grießinger:** Conceptualization, Writing – original draft, Writing – review & editing.

Declaration of Competing Interest

The authors declare no conflict of interest.

Data availability

Our data and results are available to everyone interested in our research.

Acknowledgments

We would like to thank three anonymous reviewers and the journal editor Prof. Howard Falcon-Lang, for the useful comments and contributions, which helped to improve the original manuscript.

Appendix A. Supplementary data

Supplementary data to this article can be found online at https://doi.org/10.1016/j.palaeo.2023.111474.

References

Abram, N.J., Mulvaney, R., Vimeux, F., Phipps, S.J., Turner, J., England, M.H., 2014. Evolution of the Southern Annular Mode during the past millennium. Nat. Clim. Chang. 4, 564–569. https://doi.org/10.1038/nclimate2235.

Aceituno, P., 1988. On the Functioning of the Southern Oscillation in the South American Sector. Part I: Surface climate. Mon. Weather Rev. 116, 505–524. https://doi.org/10.1175/1520-0493(1988)116<0505:OTFOTS>2.0.CO;2.

Aguirre, F., Carrasco, J., Sauter, T., Schneider, C., Gaete, K., Garín, E., Adaros, R., Butorovic, N., Jaña, R., Casassa, G., 2018. Snow Cover Change as a Climate Indicator in Brunswick Peninsula, Patagonia. Front, Earth Sci, (Lausanne) 6. https://doi.org/10.3389/feart.2018.00130.

Aravena, J.C., Lara, A., Wolodarsky-Franke, A., Villalba, R., Cuq, E., 2002. Tree-ring growth patterns and temperature reconstruction from *Nothofagus pumilio* (*Fagaceae*) forests at the upper tree line of southern chilean Patagonia. Rev. Chil. Hist. Nat. 75, 361–376. https://doi.org/10.4067/S0716-078X2002000200008.

Bahamonde, H.A., Sánchez-Gómez, D., Gyenge, J., Peri, P.L., Cellini, J.M., Aranda, I., 2019. Thinking in the sustainability of *Nothofagus Antarctica* silvopastoral systems, how differ the responses of seedlings from different provenances to water shortage? Agrofor. Syst. 93, 689–701. https://doi.org/10.1007/s10457-017-0167-5.

Balting, D.F., Ionita, M., Wegmann, M., Helle, G., Schleser, G.H., Rimbu, N., Freund, M. B., Heinrich, I., Caldarescu, D., Lohmann, G., 2021. Large-scale climate signals of a european oxygen isotope network from tree rings. Clim. Past 17, 1005–1023. https://doi.org/10.5194/cp-17-1005-2021.

Barbour, M.M., Walcroft, A.S., Farquhar, G.D., 2002. Seasonal variation in $\delta^{13}C$ and $\delta^{18}O$ of cellulose from growth rings of *Pinus radiata*. Plant Cell Environ. 25, 1483–1499. https://doi.org/10.1046/j.0016-8025.2002.00931.x.

Beck, H.E., Pan, M., Miralles, D.G., Reichle, R.H., Dorigo, W.A., Hahn, S., Sheffield, J., Karthikeyan, L., Balsamo, G., Parinussa, R.M., van Dijk, A.I.J.M., Du, J., Kimball, J. S., Vergopolan, N., Wood, E.F., 2021. Evaluation of 18 satellite- and model-based soil moisture products using in situ measurements from 826 sensors. Hydrol. Earth Syst. Sci. 25, 17–40. https://doi.org/10.5194/hess-25-17-2021.

Bell, B., Hersbach, H., Simmons, A., Berrisford, P., Dahlgren, P., Horányi, A., Muñoz-Sabater, J., Nicolas, J., Radu, R., Schepers, D., Soci, C., Villaume, S., Bidlot, J., Haimberger, L., Woollen, J., Buontempo, C., Thépaut, J., 2021. The ERA5 global reanalysis: preliminary extension to 1950. Q. J. R. Meteorol. Soc. 147, 4186–4227. https://doi.org/10.1002/qj.4174.

Belmecheri, S., Wright, W.E., Szejner, P., 2022. In: Sample Collection and Preparation for Annual and Intra-annual Tree-Ring Isotope Chronologies, pp. 103–134. https://doi.org/10.1007/978-3-030-92698-4_4.

Boninsegna, J.A., Keegan, J., Jacoby, G.C., D'Arrigo, R., Holmes, R.L., 1989. Dendrochronological Studies in Tierra del Fuego. In: Quaternary of South America and Antarctic Peninsula. CRC Press, Argentina, in, pp. 315–326. https://doi.org/10.1201/9781003079361-16.

Brienen, R.J.W., Helle, G., Pons, T.L., Guyot, J.-L., Gloor, M., 2012. Oxygen isotopes in tree rings are a good proxy for Amazon precipitation and El Niño-Southern Oscillation variability. Proc. Natl. Acad. Sci. 109, 16957–16962. https://doi.org/10.1073/pnas.1205977109.

Bucci, S.J., Carbonell Silletta, L.M., Garré, A., Cavallaro, A., Efron, S.T., Arias, N.S., Goldstein, G., Scholz, F.G., 2019. Functional relationships between hydraulic traits and the timing of diurnal depression of photosynthesis. Plant Cell Environ. 42, 1603–1614. https://doi.org/10.1111/pce.13512.

Bucci, S.J., Scholz, F.G., Campanello, P.I., Montti, L., Jimenez-Castillo, M., Rockwell, F. A., Manna, L.L., Guerra, P., Bernal, P.L., Troncoso, O., Enricci, J., Holbrook, M.N., Goldstein, G., 2012. Hydraulic differences along the water transport system of South American *Nothofagus* species: do leaves protect the stem functionality? Tree Physiol. 32, 880–893. https://doi.org/10.1093/treephys/tps054.

Carrasco, J.F., 2021. La Baja del Mar de Amundsen, su variabilidad ejemplo de conexión hemisférica. Bach 40, 22–24.

Carrasco, J.F., 2013. Decadal changes in the Near-Surface Air Temperature in the Western Side of the Antarctic Peninsula. Atmos. Clim. Sci. 03, 275–281. https://doi.org/10.4236/acs.2013.33029.

Carrasco, J.F., Casassa, G., Rivera, A., 2002. In: Meteorological and Climatological Aspects of the Southern Patagonia Icefield, pp. 29–41. https://doi.org/10.1007/978-1-4615-0645-4_4.

Cook, E.R., Briffa, K.R., 1990. A comparison of some Tree-Ring Standardization Methods. In: Cook, E.R., Kairiukstis, L.A. (Eds.), Methods of Dendrochronology. Applications in the Environmental Sciences, Springer, Netherlands, Dordrecht, pp. 153–162.

Cpc, 2022. Climate Prediction Center [WWW Document]. https://www.cpc.ncep.noaa.gov/products/precip/CWlink/daily_ao_index/aao/aao.shtml.

Csank, A.Z., Miller, A.E., Sherriff, R.L., Berg, E.E., Welker, J.M., 2016. Tree-ring isotopes reveal drought sensitivity in trees killed by spruce beetle outbreaks in south-Central Alaska. Ecol. Appl. 26, 2001–2020. https://doi.org/10.1002/eap.1365.

Dätwyler, C., Neukom, R., Abram, N.J., Gallant, A.J.E., Grosjean, M., Jacques-Coper, M., Karoly, D.J., Villalba, R., 2018. Teleconnection stationarity, variability and trends of the Southern Annular Mode (SAM) during the last millennium. Clim. Dyn. 51, 2321–2339. https://doi.org/10.1007/s00382-017-4015-0.

Dmc, 2022. Dirección Meteorologica de Chile, [WWW Document]. http://www.meteochile.cl/.

Fogt, R.L., Marshall, G.J., 2020. The Southern Annular Mode: Variability, trends, and climate impacts across the Southern Hemisphere. WIREs Clim. Change 11. https://doi.org/10.1002/wcc.652.

Fogt, R.L., Perlwitz, J., Monaghan, A.J., Bromwich, D.H., Jones, J.M., Marshall, G.J., 2009. Historical SAM Variability. Part II: Twentieth-Century Variability and Trends from Reconstructions, Observations, and the IPCC AR4 Models*. J. Clim. 22, 5346–5365. https://doi.org/10.1175/2009JCLI2786.1.

Fogt, R.L., Wovrosh, A.J., Langen, R.A., Simmonds, I., 2012. The characteristic variability and connection to the underlying synoptic activity of the Amundsen-Bellingshausen Seas Low. J. Geophys. Res. Atmos. 117, n/a-n/a. https://doi.org/10.1029/2011JD017337.

Foroozan, Z., Grießinger, J., Pourtahmasi, K., Bräuning, A., 2020. 501 years of Spring Precipitation history for the Semi-Arid Northern Iran Derived from Tree-Ring $\delta^{18}O$ Data. Atmosphere (Basel) 11, 889. https://doi.org/10.3390/atmos11090889.

Fuentes, M., Aravena, J.C., Seim, A., Linderholm, H.W., 2019. Assessing the dendroclimatic potential of *Nothofagus betuloides* (Magellan's beech) forests in the southernmost chilean Patagonia. Trees 33, 557–575. https://doi.org/10.1007/s00468-018-1801-1.

Garreaud, R., 2018. Record-breaking climate anomalies lead to severe drought and environmental disruption in western Patagonia in 2016. Clim. Res. 74, 217–229. https://doi.org/10.3354/cr01505.

Garreaud, R., Clem, K., Veloso, J.V., 2021. The South Pacific pressure Trend Dipole and the Southern Blob. J. Clim. 34, 7661–7676. https://doi.org/10.1175/JCLI-D-20-0886.1.

Garreaud, R., Lopez, P., Minvielle, M., Rojas, M., 2013. Large-Scale Control on the Patagonian climate. J. Clim. 26, 215–230. https://doi.org/10.1175/JCLI-D-12-00001.1.

Garreaud, R.D., Vuille, M., Compagnucci, R., Marengo, J., 2009. Present-day south american climate. Palaeogeogr. Palaeoclimatol. Palaeoecol. 281, 180–195. https://doi.org/10.1016/j.palaeo.2007.10.032.

Gessler, A., Brandes, E., Keitel, C., Boda, S., Kayler, Z.E., Granier, A., Barbour, M., Farquhar, G.D., Treydte, K., 2013. The oxygen isotope enrichment of leaf-exported assimilates – does it always reflect lamina leaf water enrichment? New Phytol. 200, 144–157. https://doi.org/10.1111/nph.12359.

Gessler, A., Ferrio, J.P., Hommel, R., Treydte, K., Werner, R.A., Monson, R.K., 2014. Stable isotopes in tree rings: towards a mechanistic understanding of isotope fractionation and mixing processes from the leaves to the wood. Tree Physiol. 34, 796–818. https://doi.org/10.1093/treephys/tpu040.

González-Reyes, Á., Aravena, J.C., Muñoz, A.A., Soto-Rogel, P., Aguilera-Betti, I., Toledo-Guerrero, I., 2017. Variabilidad de la precipitación en la ciudad de Punta Arenas, Chile, desde principios del siglo XX. Anales del Instituto de la Patagonia 45, 31–44. https://doi.org/10.4067/S0718-686X2017000100031.

Grießinger, J., Langhamer, L., Schneider, C., Saß, B.-L., Steger, D., Skvarca, P., Braun, M. H., Meier, W.J.-H., Srur, A.M., Hochreuther, P., 2018. Imprints of climate Signals in a 204 year δ18O Tree-Ring Record of *Nothofagus pumilio* from Perito Moreno Glacier, Southern Patagonia (50°S). Front. Earth Sci. (Lausanne) 6. https://doi.org/10.3389/feart.2018.00027.

Hersbach, H., Bell, B., Berrisford, P., Hirahara, S., Horányi, A., Muñoz-Sabater, J., Nicolas, J., Peubey, C., Radu, R., Schepers, D., Simmons, A., Soci, C., Abdalla, S., Abellan, X., Balsamo, G., Bechtold, P., Biavati, G., Bidlot, J., Bonavita, M., Chiara, G., Dahlgren, P., Dee, D., Diamantakis, M., Dragani, R., Flemming, J., Forbes, R., Fuentes, M., Geer, A., Haimberger, L., Healy, S., Hogan, R.J., Hólm, E., Janisková, M., Keeley, S., Laloyaux, P., Lopez, P., Lupu, C., Radnoti, G., Rosnay, P., Rozum, I., Vamborg, F., Villaume, S., Thépaut, J., 2020. The ERA5 global reanalysis. Q. J. R. Meteorol. Soc. 146, 1999–2049. https://doi.org/10.1002/qj.3803.

Hosking, J.S., Orr, A., Marshall, G.J., Turner, J., Phillips, T., 2013. The Influence of the Amundsen-Bellingshausen Seas Low on the climate of West Antarctica and its Representation in coupled climate Model Simulations. J. Clim. 26, 6633–6648. https://doi.org/10.1175/JCLI-D-12-00813.1.

Iogna, P.A., Bucci, S.J., Scholz, F.G., Goldstein, G., 2013. Homeostasis in leaf water potentials on leeward and windward sides of desert shrub crowns: water loss control

vs. high hydraulic efficiency. Oecologia 173, 675–687. https://doi.org/10.1007/s00442-013-2666-z.
Jacques-Coper, M., Brönnimann, S., Martius, O., Vera, C., Cerne, B., 2016. Summer heat waves in southeastern Patagonia: an analysis of the intraseasonal timescale. Int. J. Climatol. 36, 1359–1374. https://doi.org/10.1002/joc.4430.
Knmi, 2022. Climate Explorer [WWW Document]. http://climexp.knmi.nl/.
Kress, A., Saurer, M., Siegwolf, R.T.W., Frank, D.C., Esper, J., Bugmann, H., 2010. A 350 year drought reconstruction from Alpine tree ring stable isotopes. Glob. Biogeochem. Cycles 24, n/a-n/a. https://doi.org/10.1029/2009GB003613.
Labuhn, I., Daux, V., Girardclos, O., Stievenard, M., Pierre, M., Masson-Delmotte, V., 2016. French summer droughts since 1326 CE: a reconstruction based on tree ring cellulose $\delta^{18}O$. Clim. Past 12, 1101–1117. https://doi.org/10.5194/cp-12-1101-2016.
Laumer, W., Andreu, L., Helle, G., Schleser, G.H., Wieloch, T., Wissel, H., 2009. A novel approach for the homogenization of cellulose to use micro-amounts for stable isotope analyses. Rapid Commun. Mass Spectrom. 23, 1934–1940. https://doi.org/10.1002/rcm.4105.
Lavergne, A., Daux, V., Villalba, R., Pierre, M., Stievenard, M., Vimeux, F., Srur, A.M., 2016. Are the oxygen isotopic compositions of *Fitzroya cupressoides* and *Nothofagus pumilio* cellulose promising proxies for climate reconstructions in northern Patagonia? J. Geophys. Res. Biogeosci. 121, 767–776. https://doi.org/10.1002/2015JG003260.
Llancabure, J.C., 2011. Relaciones entre el crecimiento de *Nothofagus betuloides* y el clima Local y de gran escala en bosques subantárticos de la Isla Navarino (Bachelor's Thesis). Universidad Austral de Chile, Valdivia, Chile.
Marshall, G.J., 2003. Trends in the Southern Annular Mode from Observations and Reanalyses. J. Clim. 16, 4134–4143. https://doi.org/10.1175/1520-0442(2003)016<4134:TITSAM>2.0.CO;2.
Marshall, J.D., Monserud, R.A., 2006. Co-occurring species differ in tree-ring ^{18}O trends. Tree Physiol. 26, 1055–1066. https://doi.org/10.1093/treephys/26.8.1055.
Matskovsky, V., Roig, F.A., Fuentes, M., Korneva, I., Araneo, D., Linderholm, H.W., Aravena, J.C., 2022. Summer temperature changes in Tierra del Fuego since AD 1765: atmospheric drivers and tree-ring reconstruction from the southernmost forests of the world. Clim. Dyn. https://doi.org/10.1007/s00382-022-06384-0.
Meier, W.J.-H., Aravena, J.-C., Jaña, R., Braun, M.H., Hochreuther, P., Soto-Rogel, P., Grießinger, J., 2020. A tree-ring $\delta^{18}O$ series from southernmost Fuego-Patagonia is recording flavors of the Antarctic Oscillation. Glob. Planet. Change 195. https://doi.org/10.1016/j.gloplacha.2020.103302.
Muñoz-Sabater, J., Dutra, E., Agustí-Panareda, A., Albergel, C., Arduini, G., Balsamo, G., Boussetta, S., Choulga, M., Harrigan, S., Hersbach, H., Martens, B., Miralles, D.G., Piles, M., Rodríguez-Fernández, N.J., Zsoter, E., Buontempo, C., Thépaut, J.-N., 2021. ERA5-Land: a state-of-the-art global reanalysis dataset for land applications. Earth Syst. Sci. Data 13, 4349–4383. https://doi.org/10.5194/essd-13-4349-2021.
Nagavciuc, V., Ionita, M., Perşoiu, A., Popa, I., Loader, N.J., McCarroll, D., 2019. Stable oxygen isotopes in Romanian oak tree rings record summer droughts and associated large-scale circulation patterns over Europe. Clim. Dyn. 52, 6557–6568. https://doi.org/10.1007/s00382-018-4530-7.
Naulier, M., Savard, M.M., Bégin, C., Gennaretti, F., Arseneault, D., Marion, J., Nicault, A., Bégin, Y., 2015. A millennial summer temperature reconstruction for northeastern Canada using oxygen isotopes in subfossil trees. Clim. Past 11, 1153–1164. https://doi.org/10.5194/cp-11-1153-2015.
Pisano, E., 1977. Fitogeografía de Fuego-Patagonia chilena I- Comunidades vegetales entre las latitudes 52 y 56 s. An. Inst. Patagon. 8, 121–250.
Polvani, L.M., Waugh, D.W., Correa, G.J.P., Son, S.-W., 2011. Stratospheric ozone Depletion: the Main driver of Twentieth-Century Atmospheric Circulation changes in the Southern Hemisphere. J. Clim. 24, 795–812. https://doi.org/10.1175/2010JCLI3772.1.
Porter, T.J., Pisaric, M.F.J., Field, R.D., Kokelj, S.V., Edwards, T.W.D., deMontigny, P., Healy, R., LeGrande, A.N., 2014. Spring-summer temperatures since AD 1780 reconstructed from stable oxygen isotope ratios in white spruce tree-rings from the Mackenzie Delta, northwestern Canada. Clim. Dyn. 42, 771–785. https://doi.org/10.1007/s00382-013-1674-3.
Pumijumnong, N., Bräuning, A., Sano, M., Nakatsuka, T., Muangsong, C., Buajan, S., 2020. A 338-year tree-ring oxygen isotope record from Thai teak captures the variations in the asian summer monsoon system. Sci. Rep. 10, 8966. https://doi.org/10.1038/s41598-020-66001-0.
Raphael, M.N., Marshall, G.J., Turner, J., Fogt, R.L., Schneider, D., Dixon, D.A., Hosking, J.S., Jones, J.M., Hobbs, W.R., 2016. The Amundsen Sea Low: Variability, Change, and Impact on Antarctic climate. Bull. Am. Meteorol. Soc. 97, 111–121. https://doi.org/10.1175/BAMS-D-14-00018.1.
Rinne, K.T., Loader, N.J., Switsur, V.R., Waterhouse, J.S., 2013. 400-year May–August precipitation reconstruction for Southern England using oxygen isotopes in tree rings. Quat. Sci. Rev. 60, 13–25. https://doi.org/10.1016/j.quascirev.2012.10.048.
Roden, J.S., Lin, G., Ehleringer, J.R., 2000. A mechanistic model for interpretation of hydrogen and oxygen isotope ratios in tree-ring cellulose. Geochim. Cosmochim. Acta 64, 21–35. https://doi.org/10.1016/S0016-7037(99)00195-7.
Smith, V.C., Ennos, A.R., 2003. The effects of air flow and stem flexure on the mechanical and hydraulic properties of the stems of sunflowers *Helianthus annuus* L. J. Exp. Bot. 54, 845–849. https://doi.org/10.1093/jxb/erg068.
Soliani, C., Mattera, M.G., Marchelli, P., Azpilicueta, M.M., Dalla-Salda, G., 2021. Different drought-adaptive capacity of a native Patagonian tree species (*Nothofagus pumilio*) resulting from local adaptation. Eur. J. For. Res. 140, 1147–1161. https://doi.org/10.1007/s10342-021-01389-6.
Soto-Rogel, P., Aravena, J.-C., Meier, W.J.-H., Gross, P., Pérez, C., González-Reyes, Á., Griessinger, J., 2020. Impact of extreme weather events on aboveground net primary productivity and sheep production in the magellan region, southernmost chilean Patagonia. Geosciences (Switzerland) 10. https://doi.org/10.3390/geosciences10080318.
Soto-Rogel, P., Aravena, J.C., Villalba, R., Bringas, C., Meier, W.J.-H., Gonzalez-Reyes, Á., Grießinger, J., 2022. Two *Nothofagus* Species in Southernmost South America are Recording Divergent climate Signals. Forests 13, 794. https://doi.org/10.3390/f13050794.
Srur, A.M., Villalba, R., Villagra, P.E., Hertel, D., 2008. Influencias de las variaciones en el clima y en la concentración de C0(2) sobre el crecimiento de *Nothofagus pumilio* en la Patagonia. Rev. Chil. Hist. Nat. 81 https://doi.org/10.4067/S0716-078X2008000200007.
Tognetti, R., Lombardi, F., Lasserre, B., Cherubini, P., Marchetti, M., 2014. Tree-Ring Stable Isotopes Reveal Twentieth-Century increases in Water-Use Efficiency of *Fagus sylvatica* and *Nothofagus* spp. In Italian and chilean Mountains. PLoS One 9, e113136. https://doi.org/10.1371/journal.pone.0113136.
Treydte, K.S., Schleser, G.H., Helle, G., Frank, D.C., Winiger, M., Haug, G.H., Esper, J., 2006. The twentieth century was the wettest period in northern Pakistan over the past millennium. Nature 440, 1179–1182. https://doi.org/10.1038/nature04743.
Trouet, V., van Oldenborgh, G.J., 2013. KNMI climate Explorer: a Web-based Research Tool for High-Resolution Paleoclimatology. Tree Ring Res 69, 3–13. https://doi.org/10.3959/1536-1098-69.1.3.
Turner, J., Phillips, T., Hosking, J.S., Marshall, G.J., Orr, A., 2013. The Amundsen Sea low. Int. J. Climatol. 33, 1818–1829. https://doi.org/10.1002/joc.3558.
Varela, S.A., Gyenge, J.E., Fernández, M.E., Schlichter, T., 2010. Seedling drought stress susceptibility in two deciduous *Nothofagus* species of NW Patagonia. Trees 24, 443–453. https://doi.org/10.1007/s00468-010-0412-2.
Viale, M., Bianchi, E., Cara, L., Ruiz, L.E., Villalba, R., Pitte, P., Masiokas, M., Rivera, J., Zalazar, L., 2019. Contrasting Climates at both Sides of the Andes in Argentina and Chile. Front. Environ. Sci. 7 https://doi.org/10.3389/fenvs.2019.00069.
Villalba, R., Lara, A., Boninsegna, J.A., Masiokas, M., Delgado, S., Aravena, J.C., Roig, F. A., Schmelter, A., Wolodarsky, A., Ripalta, A., 2003. Large-Scale Temperature changes across the Southern Andes: 20th-Century Variations in the Context of the past 400 years. Clim. Chang. 59, 177–232. https://doi.org/10.1023/A:1024452701153.
Villalba, R., Lara, A., Masiokas, M.H., Urrutia, R., Luckman, B.H., Marshall, G.J., Mundo, I.A., Christie, D.A., Cook, E.R., Neukom, R., Allen, K., Fenwick, P., Boninsegna, J.A., Srur, A.M., Morales, M.S., Araneo, D., Palmer, J.G., Cuq, E., Aravena, J.C., Holz, A., LeQuesne, C., 2012. Unusual Southern Hemisphere tree growth patterns induced by changes in the Southern Annular Mode. Nat. Geosci. 5, 793–798. https://doi.org/10.1038/ngeo1613.
Vuille, M., Franquist, E., Garreaud, R., Lavado Casimiro, W.S., Cáceres, B., 2015. Impact of the global warming hiatus on andean temperature. Journal of Geophysical Research: Atmospheres 120, 3745–3757. https://doi.org/10.1002/2015JD023126.
Wang, L., Liu, Y., Li, Q., Song, H., Cai, Q., 2022. Tree-ring oxygen isotope recorded precipitation variations over the past two centuries in the northeast Chinese Loess Plateau. Int. J. Climatol. https://doi.org/10.1002/joc.7562.
Wieloch, T., Helle, G., Heinrich, I., Voigt, M., Schyma, P., 2011. A novel device for batch-wise isolation of α-cellulose from small-amount wholewood samples. Dendrochronologia (Verona) 29, 115–117. https://doi.org/10.1016/j.dendro.2010.08.008.
Wigley, T.M.L., Briffa, K.R., Jones, P.D., 1984. Average value of correlated time series, with applications in dendroclimatology and hydrometeorology. J. Appl. Meteorol. 1962 (23), 201–234.
Xu, G., Liu, X., Qin, D., Chen, T., Wang, W., Wu, G., Sun, W., An, W., Zeng, X., 2014. Tree-ring δ18O evidence for the drought history of eastern Tianshan Mountains, Northwest China since 1700 AD. Int. J. Climatol. 34, 3336–3347. https://doi.org/10.1002/joc.3911.
Zhu, H., Huang, R., Asad, F., Liang, E., Bräuning, A., Zhang, X., Dawadi, B., Man, W., Grießinger, J., 2021. Unexpected climate variability inferred from a 380-year tree-ring earlywood oxygen isotope record in the Karakoram, Northern Pakistan. Clim. Dyn. 57, 701–715. https://doi.org/10.1007/s00382-021-05736-6.